Machining effects and multi-objective optimization in Inconel 718 turning with unitary and hybrid nanofluids under MQL

Paresh Kulkarni
Vishwakarma Institute of Information Technology, Dr. D.Y. Patil Institute of Engineering, Management and Research, Pune-411044, India
paresh.219p0014@viit.ac.in, http://orcid.org/0000-0002-2761-8754

Satish Chinchanikar
Mechanical department, Vishwakarma Institute of Information Technology, Pune, India
satish.chinchanikar@viit.ac.in, http://orcid.org/0000-0002-4175-3098

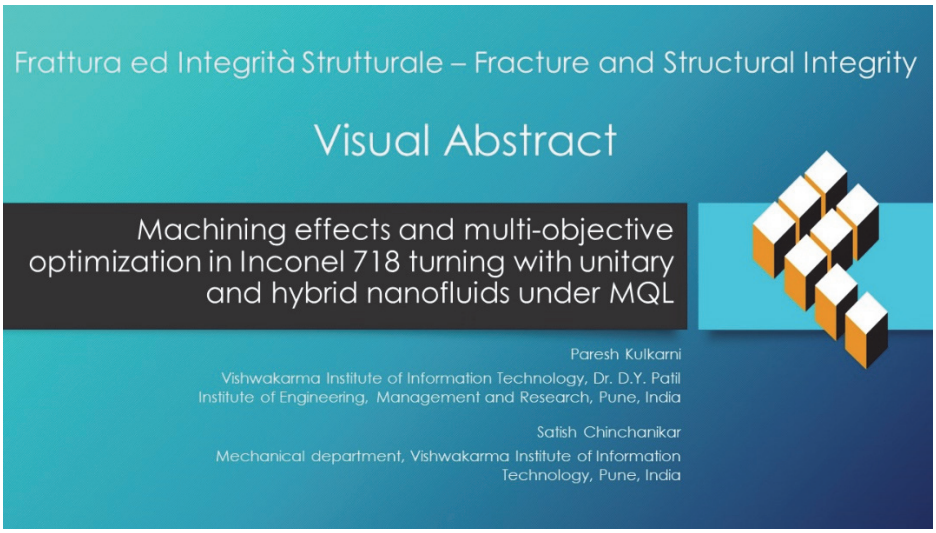

Citation: Kulkarni, P., Chinchanikar, S., Machining effects and multi-objective optimization in Inconel 718 turning with unitary and hybrid nanofluids under MQL, Frattura ed Integrità Strutturale, 68 (2024) 222-241.

Received: 13.01.2024
Accepted: 10.02.2024
Published: 11.02.2024
Issue: 04.2024

KEYWORDS. Inconel 718, Subtractive manufacturing, Tool wear, Fracture, Adhesion, Modeling.

INTRODUCTION

Inconel 718 is a nickel-based superalloy that is widely used in the aerospace, automotive, and power generation industries. It possesses exceptional mechanical properties, making it both high-strength and corrosion-resistant. However, machining this material presents a significant challenge due to its high-temperature strength, work-hardening behavior, and poor thermal conductivity. The traditional methods of machining Inconel 718 often lead to reduced tool lifespan, increased production costs, and compromised component quality [1].

When machining nickel alloys, it is crucial to choose the right process parameters to ensure sustainable machining with maximum efficiency. Numerous research works attempted the machinability of nickel alloys, which have considered process variables, the shape and material of the tool, and cooling techniques [1–2]. Using a variety of cutting tools and novel sustainable lubrication techniques, including cryogenic minimum quantity lubrication (MQL) systems, the machinability of Inconel 718 was examined. It was found to have improved effects over cutting forces, tool wear, chip morphology, energy, and poser consumptions, and so forth [3-4]. Additionally, attempts were undertaken with hybrid and homothetic micro-textured cutting tools [5-7]. These endeavors sought to enhance machining efficiency even more.

Despite flood cooling's capacity to tackle machinability issues, there are legislative restrictions on its use to reduce its health and environmental implications [2]. MQL is a feasible solution for reducing the amount of cutting fluid used and, as a result, its negative consequences. In recent years, the application of nanofluids has tremendously increased during machining operations because of their environmental and industrial sustainability. Properties such as having a lower contact angle (wettability), surface tension, viscosity, and acid value and higher heat transfer coefficient are distinctive properties of nanofluids for machining. The type of base fluid and nanoparticle(s), along with their concentration in the base fluid, also have a vital influence on the machining aspect [8]. Incorporating nanosized particles and tubes like multi-walled carbon nanotubes (MWCNT) and aluminum oxide (Al_2O_3) into a base cutting fluid like sunflower oil improves the cooling, lubricating, and heat transfer coefficient of the resulting fluid under MQL conditions to improve machinability and avoid operator health concerns [9].

Researchers assessed the machining effects of nickel alloys using nanofluids under MQL (NFMQL) conditions [10]. Faheem et al. [11] carried out the turning of Inconel 718 using Al_2O_3 and TiO_2-based nanofluids. Their study showed lower surface roughness for a concentration of one gram of Al_2O_3. Researchers attempted to enhance the heat transfer coefficient of nanofluids by dispersing different nanoparticles in a base fluid (hybrid nanofluid). To improve the MQL performance, Sharma et al. [12] used hybrid nanofluid-based lubrication for near-dry machining, adding silicon carbide (SiC) and hexagonal boron nitride (hBN) nanoparticles.

Machine learning and data science algorithms are being utilized in the manufacturing sector to predict and optimize various industrial processes [13-14]. The integration of artificial intelligence (AI) techniques is being explored as a promising method to tackle machining challenges in cutting challenging alloys. Artificial neural networks (ANN) and adaptive neuro-fuzzy inference systems (ANFIS), has significantly impacted various industrial processes, including machining, by offering data-driven insights and predictive capabilities. The desirability function approach was utilized to evaluate the machinability of Inconel 718 [15]. The study indicated that the combination of a specific coated cutting insert and machining parameters led to optimal performance.

The Inconel 718 machining using nanofluids was analyzed, modeled, and optimized using ANN, ANFIS, and genetic programming (GP) methods. When compared to ANN and ANFIS, the GP models predicted the machining characteristics with the highest accuracy [16]. Several attempts were made to predict the optimal machining parameters for Inconel 718 using hybrid machine learning (ML) models and evolutionary algorithms [17-18]. The multi-criteria decision-making (MCDM) methods were widely utilized to derive a single solution out of multiple evolutionary algorithms solutions [19-20]. To get over the drawbacks of gray relational analysis (GRA), the optimization of the Inconel 718 milling employed several multi-objective approaches. This led to the optimization of the gray relational grade (GRG) with a single purpose. It was demonstrated that GRG performed more effectively in terms of efficacy than traditional GRA models [21]. Inconel 690 milling severely damages cutting tools because of its low heat conductivity and poor machinability, which raises manufacturing costs. A three-phase computational method was used to determine the optimum tradeoff solution was used to optimize the Inconel 690 milling operations [22]. The outcomes demonstrated notable gains in efficiency, precision, and economy of cost.

From the literature review, very few attempts have been observed on the machining of Inconel 718 using unitary and hybrid nanofluids under MQL. Moreover, very few studies correlated machining performance with the properties of nanofluids. With this view, the present study investigates the machining performance during the turning of Inconel 718 using nanofluids under minimum quantity lubrication (NFMQL) through mathematical modeling and multi-objective optimization. Nanofluids were prepared by mixing unitary aluminum oxide (Al_2O_3) and combination of nanoparticles such as aluminium oxide+multi-walled carbon nanotubes (Al_2O_3+MWCNT) at constant proportions in vegetable-based palm oil. The prepared nanofluids are characterized in terms of thermal conductivity, wettability, surface tension, viscosity, pH value, and density. The worn-out tools were analyzed through images captured using optical and scanning electron microscopes. A Pareto-based hybrid multi-objective technique was used to optimize the cutting parameters. The technique for order of preference by similarity to ideal solution (TOPSIS) and the genetic algorithm (GA) were combined to produce Pareto solutions and select the best compromise solution. The genetic algorithm was employed to explore the search space and generate a diverse set of solutions, while TOPSIS helped in ranking these solutions based on their proximity to the ideal compromise solution.

EXPERIMENTAL DESIGN

Turning experiments were conducted on a CNC lathe to comprehend and explore the machining effects of the unitary and hybrid nanofluids under MQL (NFMQL) (Fig. 1). Tab. 1 depicts the levels of cutting and MQL parameters that were used in the present study. The process parameters for the chosen workpiece-tool pair were carefully selected after a thorough literature review, pilot tests, machine capacity, and tool manufacturer advice. Inconel 718 with diameters of 70 mm, lengths of 400 mm, and a hardness of 37 HRC were used in these tests. Tab. 2 depicts the chemical composition of different elements in wt% of Inconel 718.

Parameter	Value	Comment
Cutting speed (V) (m/min)	30, 45, 65, 85, 100	In total, 15 experiments were conducted using a central composite rotatable design test matrix with an alpha value of 1.6817, without any repetitions. The process parameters were altered at five different levels, which included the axial points of plus and minus alpha, factorial points of plus and minus one, and the center point
Feed (f) (mm/rev)	0.1, 0.15, 0.2, 0.25, 0.3	
Depth of cut (d) (mm)	0.2, 0.3, 0.5, 0.7, 0.8	
MQL flow rate	50 ml/min	
Standoff distance	20 mm	
Nozzle diameter and angle	2 mm, 30°	
Air pressure	4 Bar	

Table 1: Process parameters for turning Inconel 718 under NFMQL.

C	Si	Mn	P	S	Cr	Mo	Ni	Al	Co	Nb+Ta	Ti	B	Fe
0.005	0.056	0.062	0.008	0.007	18.37	2.87	52.82	0.35	0.22	5.01	1.10	0.001	Bal.

Table 2: Percentage composition of different elements of Inconel 718.

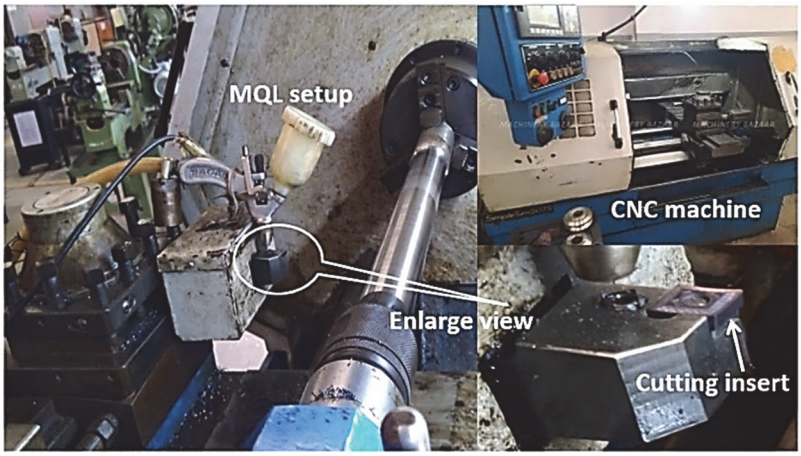

Figure 1: Experimental set-up.

The machining effects such as cutting forces, surface roughness, chip morphology, tool life, and tool wear analysis were studied. A strain gauge-type dynamometer that had been previously calibrated was used to measure the tangential cutting, feed, and radial forces. After each cutting pass, the flank wear was measured using a Dino-Lite digital microscope, and the average surface roughness (*Ra*) was measured using a Mitutoyo SJ.201 surface roughness tester. The tool life criteria were set at 0.2 mm flank wear, or a catastrophic failure, following ISO 3685-1977(E) guidelines. The experiments were performed with a PVD-AlTiN-coated carbide tool. Details of the cutting insert and a right-handed tool holder are depicted in Fig. 2. Based on a review of the relevant literature, pilot experiments, and advice from the tool's maker, the input variable ranges were chosen. These input variable ranges were selected to ensure optimal cutting performance and minimize tool wear.

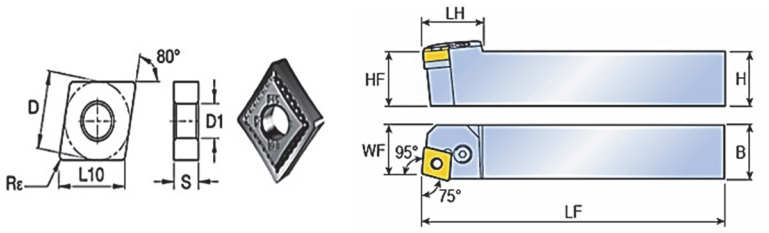

	Insert particulars					Tool holder particulars					
Parameter	D	L10	D1	S	R_c	HF	H	B	LF	LH	WF
Dimension (mm)	12.7	12.9	5.16	4.76	0.8	25	25	25	150	28	22.5

Figure 2: Cutting insert (CNMG120408MS) and tool holder (PCBNR2525M12) geometry.

Unitary and hybrid nanofluids

The use of ample amounts of cutting fluids is detrimental to the environment; however, when employing the MQL approach, just a tiny portion of base fluid is used. Nanoparticle(s) addition to the base fluid can considerably improve heat-carrying and lubricating characteristics. A mist-form of cutting fluid, i.e., a mixture of compressed air and nanofluid, is delivered to the cutting zone with a view to maintaining environmental sustainability.

The type of nanoparticles and their concentration significantly affect the wetting and thermophysical characteristics of nanofluids. Most of the studies reported that a concentration of 0.25 wt% in a base fluid produces better properties for nanofluids and, hence, better machining performance. Researchers observed improved thermal conductivity, stability, and, hence, better machining performance with Al_2O_3 and Al_2O_3+MWCNT nanoparticles when mixed in a base fluid [2, 8]. However, the optimal concentration of nanoparticles may vary depending on the application and machining conditions. Additionally, the choice of nanoparticles should also consider factors such as cost, availability, and potential environmental impacts.

In the present study, nanofluids are obtained by mixing 99% pure multi-walled carbon nanotubes (MWCNT), which had dimensions of 5 m in length and outer and inner diameters of 10–30 nm and 5–10 nm, respectively, and 99.9% pure aluminum oxide (Al_2O_3) nanoparticles, which had an average particle size of 20–50 nm, in palm oil. The high purity of the MWCNT and Al_2O_3 ensured minimal impurities that could affect the performance of the nanofluids.

The unitary Al_2O_3 nanofluid is obtained by mixing Al_2O_3 nanoparticles with a concentration of 0.25 wt% in a vegetable-based palm oil (base fluid). And MWCNT and Al_2O_3 were suspended in vegetable-based palm oil in a 50–50% proportion with a 0.25% concentration to form a hybrid Al_2O_3+MWCNT nanofluid. The pre-dispersed nanofluid was then mechanically stirred for 20 minutes at 700 rpm to ensure solution homogeneity. Probe sonication was used for about 30 minutes at a maximum frequency of 50 kHz to dilute and stir the nanoparticles in the base fluid and increase the fluid's homogeneity. To obtain further homogeneity and avoid sedimentation, the nanofluid was then magnetically stirred for 20 minutes at 500 rpm. After the magnetic stirring, the nanofluid was allowed to settle for 10 minutes to ensure any remaining air bubbles were eliminated. Finally, the homogenized nanofluid was ready for further analysis and experimentation. To improve the dispersion and stability of the nanofluids, sodium dodecyl sulfate was used as a surfactant to lessen the agglomeration of nanoparticles. This surfactant also played a crucial role in preventing the nanoparticles from settling down over time, ensuring long-term stability [23]. The typical standard two-step method was utilized for the preparation of nanofluid, as depicted in Fig. 3.

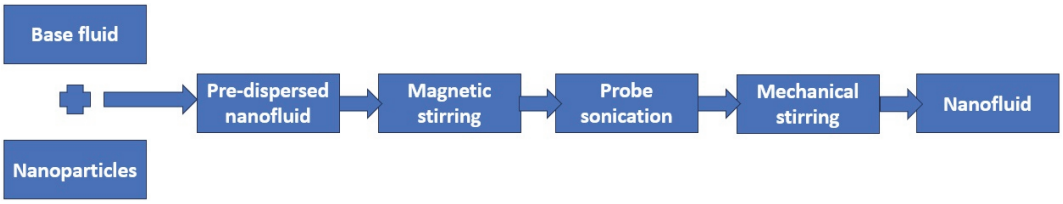

Figure 3: Two-step method for nanofluid preparation.

The measured characteristics of unitary and hybrid nanofluids are depicted in Tab. 3. The hybrid nanofluid exhibits enhanced viscosity and better thermal conductivity and heat transfer properties compared to the base fluid. This

improvement can be attributed to the synergistic effects of combining Al_2O_3 and MWCNT nanoparticles in the base fluid. The hybrid Al_2O_3+MWCNT nanofluid is a promising option for a variety of applications requiring effective lubrication and heat dissipation due to its increased viscosity, thermal conductivity, and heat transfer properties.

Type of nanofluid	Nanofluid characteristics					
	Density (g/ml)	Viscosity (cP)	Acid value (KOH/g)	Surface tension (N/m)	Contact angle (°)	Thermal conductivity (W/m°C)
Unitary Al_2O_3	0.945	38	8.77	48.81	23.3	0.254
Hybrid Al_2O_3+MWCNT	0.945	212	4.61	43.02	32.55	0.213

Table 3: Characteristics of unitary and hybrid nanofluids used in the present study.

METHODOLOGY

Exploring the heterogeneous regions of the solution space is possible with a multi-objective genetic algorithm (MOGA). The Pareto fronts are used to depict MOGA solutions. Different sets of optimum outcomes are obtained after the genetic optimization. Nevertheless, it also becomes necessary to obtain the best results for each identified optimized response. Therefore, to rank the optimal responses, multi-criteria decision-making, or MCDM, becomes crucial. This section explores the use of a hybrid Pareto-based multi-objective technique, the GA-TOPSIS method, to find the best combination of cutting parameters to achieve the required machining performance. The present hybrid optimization approach (GA-TOPSIS) evaluates the trade-offs between process responses to determine the ideal operating parameters for turning Inconel 718 alloy. The GA was used to search the space and produce a variety of solutions, and TOPSIS assisted in ranking these solutions according to how closely they matched the optimal compromise solution.

The TOPSIS method is commonly utilized for solving multi-criteria decisions, involving the identification of both positive and negative ideal solutions [24-27]. The best alternative solution is identified as the value that is nearest to the positive ideal solution (PIS), and the worst alternative solution is identified as the value that is nearest to the negative ideal solution (NIS); hence, a collection of values will define the ranking system. The benefit function requirements are raised and the cost function criteria are lowered in the case of PIS, while the opposite is true for NIS. The PIS and NIS are used to determine the segregation values at this stage. Using the Euclidean distance concept, these separation measure values are evaluated. The relative proximity values are used to determine the ranking. The value nearest to 1 represents the first rank, which is referred to as the ideal solution. The number nearest to zero represents the worst solution.

The responses are first normalized using Eqn. (1) to initiate the TOPSIS step-by-step procedure. The second phase involves computing the weighted normalized responses using Eqn. (2). Next, in the third phase, Eqns. (3) and (4) are to be used to generate the PIS and NIS. The separation of each option from PIS and NIS must then be ascertained using Eqns. (5) and (6) in the fourth phase. Lastly, use Eqn. (7) to get the closeness coefficient of each choice.

$$r_{ij} = \frac{x_{ij}}{\sqrt{\sum_{1}^{m} x_{ij}^2}} \tag{1}$$

where i = 1,2,3, - - -m; j = 1, 2, 3, - - -n

x_{ij} represents the actual value of the ith value of jth experiment. r_{ij} represents the corresponding normalized value.

$$V_{ij} = W_j \times r_{ij} \tag{2}$$

where i = 1, 2, 3, - - -m; j = 1, 2, 3, - - -n, w_j represents the weight of the j^{th} process response or criteria.

$$V^{+}=\left(v_1^{+},v_2^{+},v_3^{+},v_4^{+},---v_n^{+}\right) \tag{3}$$

$$V^{-}=\left(v_1^{-},v_2^{-},v_3^{-},v_4^{-},---v_n^{-}\right) \tag{4}$$

$$S_i^{+}=\sqrt{\sum_{j=1}^{n}\left(v_{ij}-v_j^{+}\right)^2} \tag{5}$$

$$S_i^{-}=\sqrt{\sum_{j=1}^{n}\left(v_{ij}-v_j^{-}\right)^2} \tag{6}$$

$$CC_i=\frac{S_i^{-}}{S_i^{+}+S_i^{-}} \tag{7}$$

The set of higher-ranking solutions derived from genetic optimization in a multi-objective problem is fed into a decision matrix. The created choice matrix must then be transformed into a normalized scale. This stage involves transforming the various characteristic dimensions into non-dimensional features, which enable assessment along a criterion. The cost and benefit functions are what criteria are used for. The third step involves multiplying the output parameters' weights by each column of the normalized matrix. In this study, the weights of the output parameters (responses), is obtained using the entropy weight method (EWM).

EWM is a widely used weighting method that gauges value dispersion in decision-making, with higher dispersion indicating greater differentiation and enabling more comprehensive information extraction. EWM eliminates subjective weighting models' human influence, improving objectivity. As a result, in recent years, decision-making has made extensive use of the EWM [28-30]. The weights of the output parameters are calculated as follows.

This method involves setting *m* indicators and *n* samples for the evaluation and recording the measured value of the i^{th} indicator in the j^{th} sample as x_{ij}. The initial stage is to standardize the measured values [31-32]. Using Eqn. (8), one can determine the standardized value of the i^{th} index in the j^{th} sample, which is represented as P_{ij}. Next, using Eqn. (9) [33], the entropy value E_i of the i^{th} index is found. The entropy value E_i has a range of (0, 1). Greater differentiation degree of index *i* and higher derivation of information are possible with larger E_i values. Thus, the index ought to be assigned a higher weight. As a result, Eqn. (10) is used in the EWM to determine the weight w_i [34].

$$p_{ij}=\frac{x_{ij}}{\sum_{j=1}^{n}x_{ij}} \tag{8}$$

$$E_i=\frac{\sum_{j=1}^{n}p_{ij}.\ln\left(p_{ij}\right)}{\ln(n)} \tag{9}$$

$$w_i=\frac{1-E_i}{\sum_{i=1}^{m}\left(1-E_i\right)} \tag{10}$$

RESULTS AND DISCUSSION

In this study, the turning performance of Inconel 718 was assessed considering three components of cutting force, namely the tangential cutting force (F_c), feed force (F_f), and radial force (F_r), machined surface roughness (R_a), and tool life (T), through mathematical modeling and a multi-objective optimization approach. In addition, the effects of unitary Al_2O_3 and hybrid Al_2O_3+MWCNT nanofluids on chip morphology and tool wear mechanisms under MQL circumstances were analyzed. Turning experiments were conducted under NFMQL conditions, and experimental results for unitary and hybrid nanofluids are depicted in Tab. 4.

Expt. Index	Cutting speed (V) (m/min)	Feed (f) (mm/rev)	Depth of cut (d) mm	Unitary Al_2O_3 nanofluid					Hybrid Al_2O_3+MWCNT nanofluid				
				F_c (N)	F_f (N)	F_r (N)	R_a (μm)	T (min)	F_c (N)	F_f (N)	F_r (N)	R_a (μm)	T (min)
1	65	0.2	0.8	558	277	84	1.73	2.48	537	245	77	1.49	4.21
2	45	0.15	0.7	388	226	64	1.77	5.88	431	198	68	1.36	7.70
3	45	0.25	0.7	627	316	109	2.24	3.55	617	338	108	1.9	5.46
4	85	0.15	0.7	382	167	56	1.23	2.06	374	156	48	1.15	3.01
5	85	0.25	0.7	607	287	95	1.82	1.24	568	265	76	1.78	2.14
6	65	0.2	0.5	369	139	65	1.53	2.80	277	142	47	1.42	4.06
7	65	0.1	0.5	176	79	36	1.06	5.67	168	86	33	0.93	7.18
8	65	0.3	0.5	509	258	75	1.81	2.14	473	255	71	1.88	3.29
9	30	0.2	0.5	431	164	63	2.16	11.03	343	156	56	2.06	14.14
10	100	0.2	0.5	342	128	36	1.39	1.35	313	116	38	1.15	2.08
11	45	0.15	0.3	195	69	29	1.19	10.91	166	67	31	1.02	12.91
12	45	0.25	0.3	264	118	46	1.53	6.58	248	96	34	1.82	9.15
13	85	0.15	0.3	146	69	22	0.73	3.81	136	57	26	0.94	5.05
14	85	0.25	0.3	264	95	29	1.37	2.30	234	87	34	1.32	3.58
15	65	0.2	0.2	117	59	17	1.32	6.06	107	57	24	1.02	8.09

Table 4: Experimental design and results.

Mathematical models

Mathematical models are developed to understand the parametric effect on machining performance with unitary and hybrid nanofluids. Regression equations were developed based on experimental data. The unknown coefficients in the equation were calculated using the DataFit software. Eqns. (11)-(20) presents empirical models for predicting responses during the turning of Inconel 718 alloy under NFMQL conditions. These models can be used to optimize the turning process and improve machining performance.

$$F_c = 5390.305V^{-0.1342} f^{0.9109} d^{0.9903} \tag{11}$$

$$F_f = 4230.465V^{-0.197} f^{0.9983} d^{1.2382} \tag{12}$$

$$F_r = 1706.818V^{-0.2961} f^{0.9056} d^{1.104303} \tag{13}$$

$$R_a = 25.9848V^{-0.4087} f^{0.5516} d^{0.3528} \tag{14}$$

$$T = 373.0818V^{-1.652} f^{-0.99} d^{-0.7292} \tag{15}$$

$$F_c = 4942.402V^{-0.1296} f^{0.8624} d^{1.1279} \quad (16)$$

$$F_f = 7211.217V^{-0.2775} f^{1.1512} d^{1.2737} \quad (17)$$

$$F_r = 1834.879V^{-0.3678} f^{0.8298} d^{1.0636} \quad (18)$$

$$R_a = 28.5141V^{-0.3952} f^{0.7459} d^{0.2311} \quad (19)$$

$$T = 474.7926V^{-1.4754} f^{-0.6737} d^{-0.6089} \quad (20)$$

R-squared is a statistical coefficient that measures the proportion of variation in data, with a significant equation indicating a value close to one. The developed models have R-squared values close to 0.9, indicating their reliability in predicting responses during the turning of Inconel 718 using unitary, Eqns. (11) to (15), and hybrid nanofluids, Eqns. (16) to (20), under MQL conditions. The equations are valid within the chosen parameters for the given tool and workpiece pair combination in the present study.

The plots are created using empirical equations to analyze the influence of input parameters on machining performance. Plots are produced by varying a single process parameter at a time while taking other parameters' central values into account (Tab. 1). This approach allows for a systematic analysis of the impact of each process parameter on the overall outcome. By isolating one parameter at a time, it becomes easier to understand its individual influence and make informed decisions based on the observed trends. Fig. 4 depicts plots of cutting forces during the turning of Inconel 718 alloy using unitary Al_2O_3 nanofluid (U-type) and hybrid Al_2O_3+MWCNT nanofluid (H-type) under MQL plotted using Eqns. (11)-(15) and Eqns. (16)-(20), respectively.

Fig. 4(a) depicts the plot of cutting forces varying with the cutting speed and at a constant feed and depth of cut of 0.2 mm/rev and 0.5 mm, respectively. It is possible that the material softened by the higher cutting temperature during machining is the cause of the reduced cutting forces seen at higher cutting speeds. This softening of the material reduces its resistance to deformation, resulting in lower cutting forces. Additionally, the increase in cutting speed promotes the formation of a thinner and more stable chip and its better evacuation, reducing the contact between the tool and the workpiece, which further contributes to lower cutting forces.

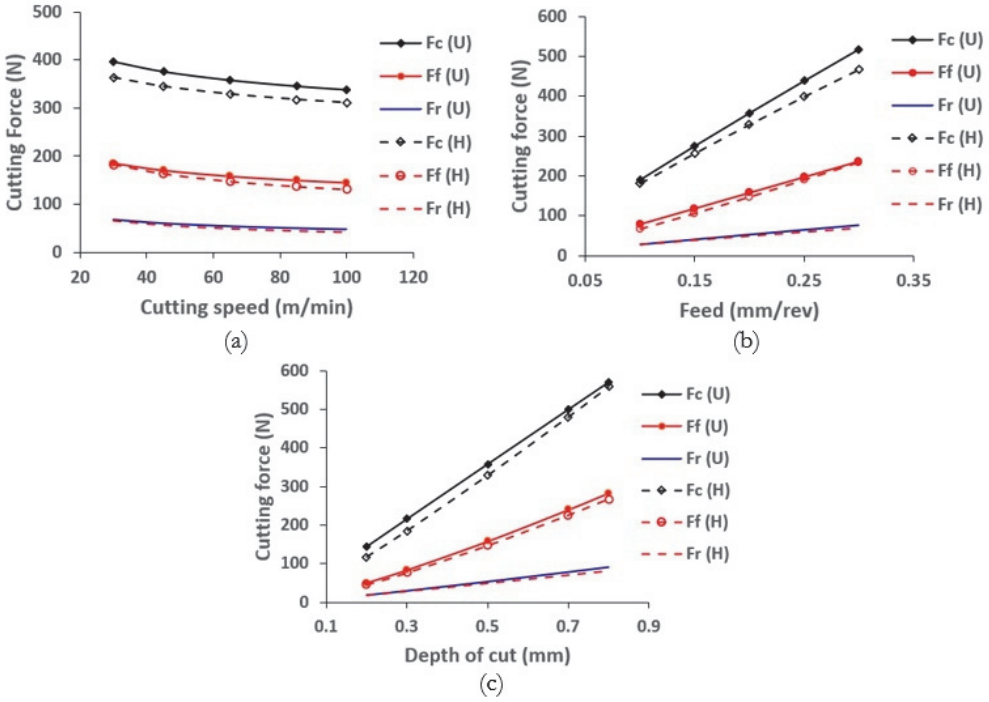

Figure 4: Cutting forces for unitary and hybrid nanofluids varying with (a) V, (b) f, and (c) d.

Figs. 4(b) and (c), respectively, show how the cutting forces increase as the feed and depth of cut increase. In contrast to feed and cutting speed, cutting forces appear to vary more noticeably with the depth of cut. This is because the depth of cut directly affects the amount of material being removed, resulting in a greater impact on cutting forces. Additionally, changes in the depth of cut can result in alterations to chip thickness and contact area, further influencing the magnitude of cutting forces. In contrast, changes in feed and cutting speed have a relatively smaller influence on cutting forces as they primarily affect the rate at which material is removed. The cutting parameters, however, appear to have a greater impact on the tangential cutting force.

The cutting forces are seen to be larger for unitary nanofluid in comparison to hybrid nanofluid, to decrease with an increase in cutting speed, and to increase with an increase in feed and depth of cut. On the other hand, it is evident that the cutting forces, particularly the tangential cutting force, increase with depth of cut, followed by feed and cutting speed. The higher positive exponent values for the depth of cut, feed, and cutting speed, in that order, are in Eqns. (11)-(13) for unitary nanofluid and Eqns. (16)-(18) for hybrid nanofluid also support this. These findings suggest that the depth of cut has a stronger impact on cutting forces than the cutting speed and feed. Additionally, the use of a unitary nanofluid results in higher cutting forces compared to a hybrid nanofluid, indicating that the type of nanofluid used can also impact cutting performance.

Lower cutting forces can be seen for hybrid nanofluids in comparison to unitary nanofluids. This could be attributed to the higher viscosity of hybrid Al_2O_3+MWCNT nanofluid compared to unitary Al_2O_3 nanofluid, as depicted in Tab. 3. The higher viscosity of hybrid nanofluid offered a lower coefficient of friction and better lubrication properties to flowing chips, which lowered the cutting forces compared to unitary nanofluid. The presence of MWCNTs in the hybrid nanofluid contributed to improved lubrication properties due to their unique structure and ability to form a protective layer on the cutting tool surface. This protective layer reduced the contact between the workpiece and the cutting tool, resulting in lower friction and cutting forces. The hybrid nanofluid demonstrated superior thermal conductivity compared to the unitary nanofluid, enhancing its cooling and lubrication capabilities during machining processes. These findings suggest that hybrid nanofluids have the potential to enhance machining processes by reducing cutting forces and improving tool life.

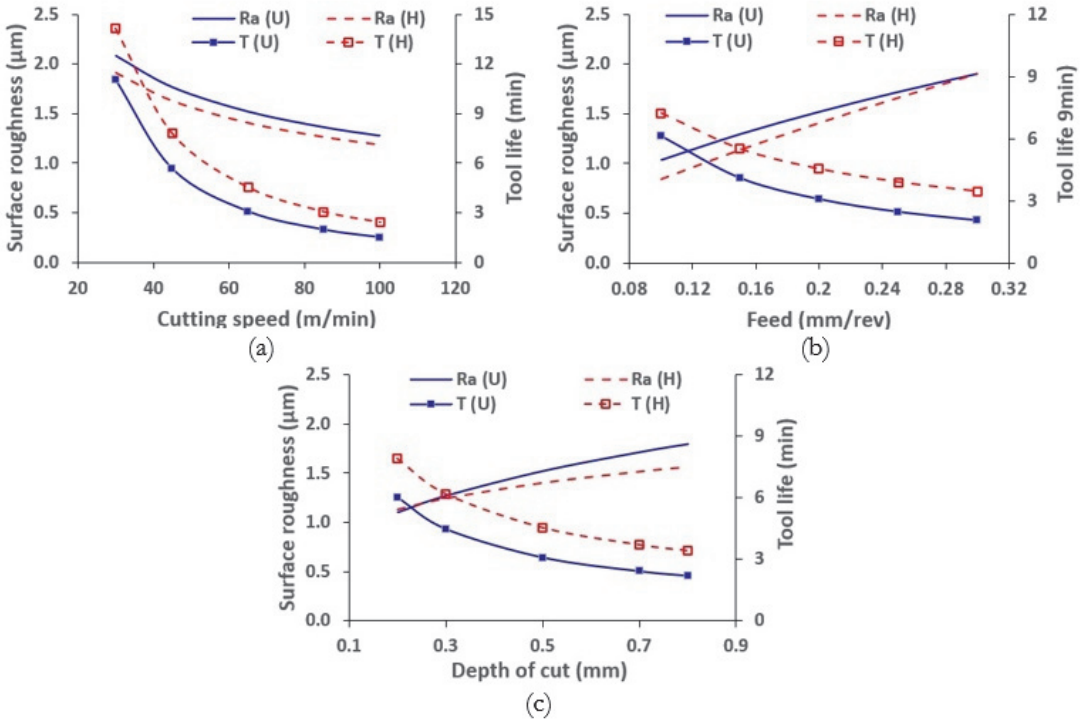

Figure 5: Surface roughness and tool life for unitary and hybrid nanofluids varying with (a) *V*, (b) *f*, and (c) *d*.

Figs. 5(a)–(c) provide plots of surface roughness and tool life as a function of cutting parameters, namely *V*, *f*, and *d*. Plots are produced by varying a single process parameter at a time while taking other parameters' central values into account (Tab. 1). This method enables a systematic analysis of each process parameter's impact on the overall outcome, enabling informed decision-making based on observed trends. Plots for surface roughness are plotted using Eqns. (14) and (19) when using

unitary and hybrid nanofluids, respectively. And plots for tool life are plotted using Eqns. (15) and (20) when using unitary and hybrid nanofluids, respectively. These equations allow for a comprehensive analysis of the effects of different types of nanofluids on both surface roughness and tool life. These plots help in understanding the performance characteristics of nanofluids in machining processes, aiding in the optimization of parameters for enhanced efficiency.

It is evident from Fig. 5 that as cutting speed increases, surface roughness decreases. And it rises more noticeably with feed, and the depth of cut follows. In contrast to unitary nanofluids, hybrid nanofluids appear to exhibit a more pronounced effect of this kind. It could be due to the spherical shape of Al_2O_3 nanoparticles providing a roller-bearing effect at the cutting interface. During machining, Al_2O_3 nanoparticles occupied the space between the workpiece and tool flank face, which provided lower friction due to a rolling bearing effect [8, 16]. Because of this, the cutting parameters have a minimal impact on surface roughness with unitary nanofluid as compared to hybrid nanofluid. Cutting speed causes the tool life to drastically decrease, and this is followed by feed and depth of cut. However, this effect can be seen as more prominent for unitary Al_2O_3 nanofluids as compared to hybrid Al_2O_3+MWCNT nanofluid. Hybrid nanofluid performed better than unitary nanofluid in terms of reduced cutting forces, surface roughness, and improved tool life. This could be due to the synergetic effect of MWCNTs' higher viscosity, lower surface tension, and Al_2O_3 nanoparticles' higher thermal conductivity and lower contact angle.

Tool wear analysis

Shear instability and localized deformation occurring during Inconel 718 machining negatively impact surface integrity, cutting forces, tool wear, and overall machinability. These challenges arise due to the material's high strength, low thermal conductivity, and work-hardening behavior. Additionally, the presence of intermetallic phases in Inconel 718 can lead to unpredictable chip formation and increased tool wear [35-36]. This sub-section discusses the investigation of the tool wear analysis during the turning of Inconel 718 alloy using a PVD-coated AlTiN carbide tool with unitary Al_2O_3 and hybrid Al_2O_3+MWCNT nanofluids under MQL conditions.

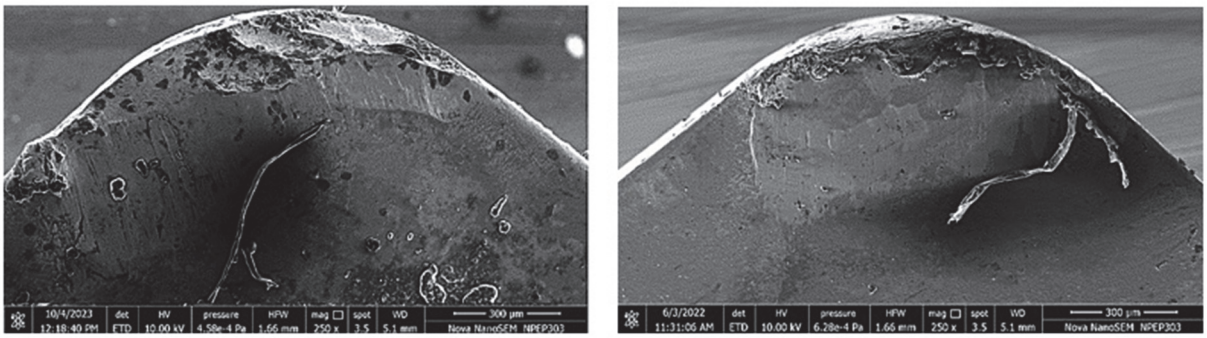

Figure 6: Tool images at experiment index 1 for (a) Unitary nanofluid, (b) Hybrid nanofluid.

The analysis of worn-out tools at different cutting conditions is discussed with the images captured using scanning electron microscopes as shown in Figs. 6-10. The photographs depict the tool's rake and flank faces upon turning at the end of the tool wear criterion, which was set at 0.2 mm of flank wear, or in the event of a catastrophic failure. A micrograph of the tools employing unitary and hybrid nanofluids at V = 65 m/min, f = 0.2 mm/rev, and d = 0.8 mm is displayed in Figs. 6(a) and (b) (experiment index 1). Severe damage to the cutting tool, coating delamination, and pitting on the substrate can be prominently seen when using unitary nanofluid. In contrast, the micrograph of the tool employing hybrid nanofluid shows significantly less damage, with minimal coating delamination and substrate pitting. Hybrid nanofluids have been found to significantly enhance the durability and performance of cutting tools compared to unitary nanofluids.

Figs. 7–10 display micrographs of tools at experiment index 7, 8, 10, and 15 using unitary and hybrid nanofluids. In almost all the cutting conditions, tool failure occurred because of metal adhesion and chipping off the cutting edge due to the breaking of the unstable piled-up adhered material during machining. This can be seen with unitary and hybrid nanofluids. However, severe metal adhesion, delamination of the coating, and edge chipping can be prominently seen for tools during the turning with unitary nanofluids under MQL cutting conditions.

The pitting on the substrate of the tool and notch wear can be seen at experiment index 7 and 8, as shown in Figs. 7 and 8. The catastrophic tool failure and chipping off the cutting edge were observed at higher cutting speeds (experiment index 10), as shown in Figs. 9(a) and (b). However, this effect appears more pronounced when using unitary nanofluids under NFMQL conditions. This shows that catastrophic tool failure and chipping off the cutting edge at higher cutting speeds

may be made more likely by using unitary nanofluid under NFMQL cutting conditions. Further investigation is required to understand the underlying mechanisms behind this phenomenon and explore potential solutions to mitigate it.

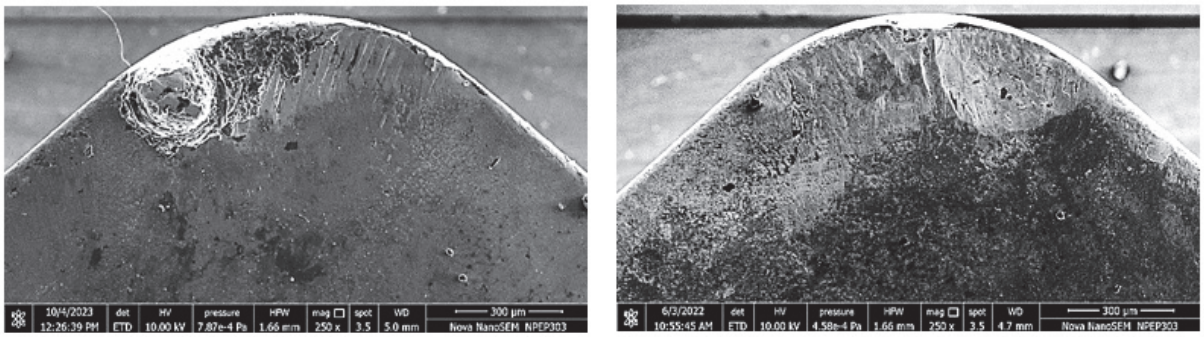

(a) (b)

Figure 7: Tool images at experiment index 7 for (a) Unitary nanofluid, (b) Hybrid nanofluid.

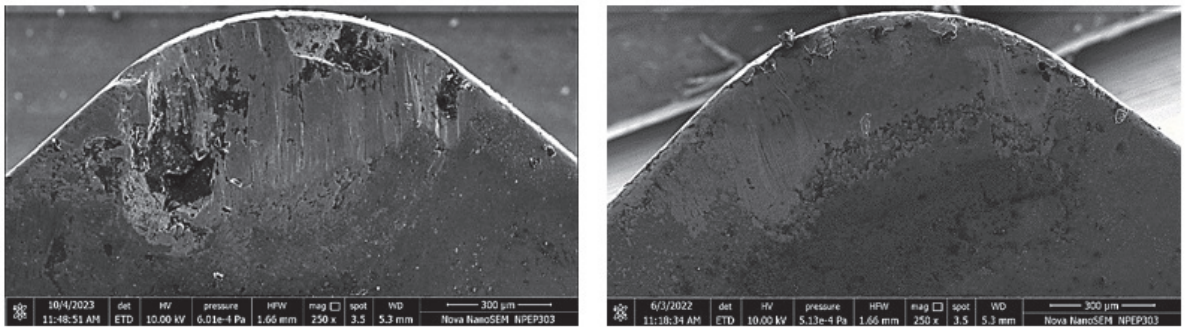

(a) (b)

Figure 8: Tool images at experiment index 8 for (a) Unitary nanofluid, (b) Hybrid nanofluid.

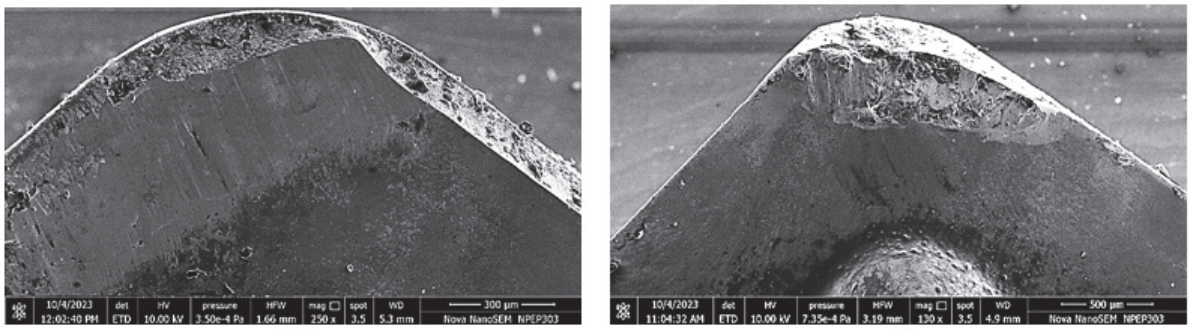

(a) (b)

Figure 9: Tool images at experiment index 10 for (a) Unitary nanofluid, (b) Hybrid nanofluid.

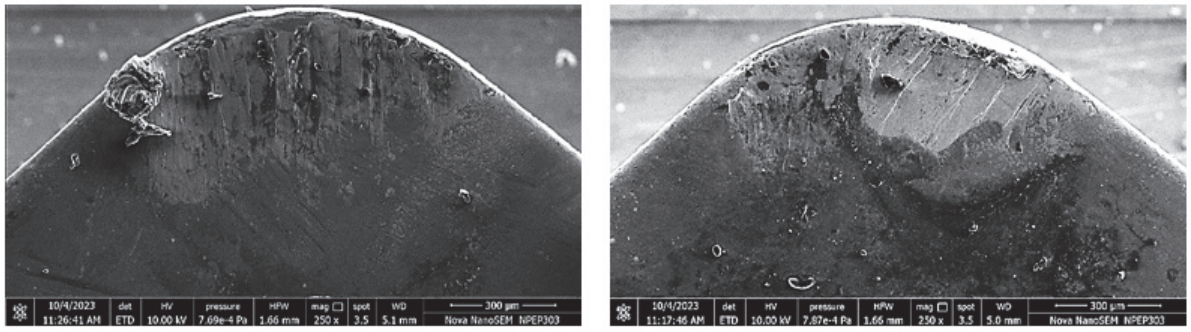

(a) (b)

Figure 10: Tool images at experiment index 15 for (a) Unitary nanofluid, (b) Hybrid nanofluid.

Chips adhering to the tool faces can be prominently seen with unitary nanofluids. The better performance of the tools with hybrid nanofluids could be attributed to their better heat-carrying capacity, which has protected the cutting tool from temperature-dependent diffusion types of wear. Hybrid nanofluids offer a lower coefficient of friction compared to unitary nanofluids, thereby reducing cutting temperatures and suppressing temperature-dependent wear mechanisms. Additionally, the improved heat-carrying capacity of hybrid nanofluids ensures more efficient cooling of the cutting tool, reducing the risk of thermal damage. This enhanced cooling capability also contributes to prolonged tool life and increased machining accuracy. Figs. 10(a) and (b) show a micrograph of the tools when using unitary and hybrid nanofluids at V = 65 m/min, f = 0.2 mm/rev, and d = 0.2 mm (experiment index 15). Severe metal adhesion, coating delamination, and pitting on the substrate can be prominently seen when using unitary nanofluid.

Nanofluids assisted in maintaining lower cutting temperatures, hence reducing abrasion risks by retaining tool hardness and preventing temperature-dependent diffusion types of wear. The study shows that built-up edge formation and adhesion wear are significant wear mechanisms when turning Inconel 718 with PVD-coated tools using unitary and hybrid nanofluids under MQL conditions. This study found that using a hybrid Al_2O_3+MWCNT nanofluid resulted in better cooling and lubricating effects, leading to a reduced tool wear rate. Compared to unitary nanofluids, the hybrid nanofluids showed the lowest tool wear for almost all the cutting conditions, which could be attributed to the synergistic effect of the better lubricating properties of MWCNTs and the roller-bearing effect of Al_2O_3 nanoparticles [8, 16]. The impact of cutting parameters on chip morphology using unitary and hybrid nanofluids under MQL is discussed in the next section.

Chip morphology

This subsection discusses the chip morphology with unitary and hybrid nanofluids under MQL. The chips formed during the machining of Inconel 718 were continuously coiled helical chips with serrated or sawtooth-type edges. Closely coiled helical chips were produced with unitary Al_2O_3 nanofluid and comparatively loosely coiled chips with hybrid Al_2O_3+MWCNT nanofluid for almost all the cutting conditions considered in this study.

The thermal conductivity of the tool and the temperature gradient between the lower temperature of the free surface and the higher temperature of the sliding surface have a major impact on chip curling [37-38]. The higher the temperature gradients between the chip's sliding and free surfaces, the lower the chip's curling radius [39]. Comparatively loosely coiled chips obtained with hybrid nanofluid show a lower temperature gradient between the chip's free and sliding surfaces, indicating better lubrication, and cooling effects by hybrid Al_2O_3+MWCNT nanofluid against unitary Al_2O_3 nanofluid.

Further, the chip with a lower curling radius, i.e., the closely coiled helical chips, is produced at higher cutting speeds and feed rates. And loosely coiled chips (with a higher curling radius) are produced at lower cutting speeds and feed rates. Higher cutting speeds lead to a greater temperature difference between the chip's sliding and free surfaces because they increase the frictional coefficient at the tool-chip contact and, therefore, the temperature. Unitary nanofluid, however, appears to have a more pronounced effect.

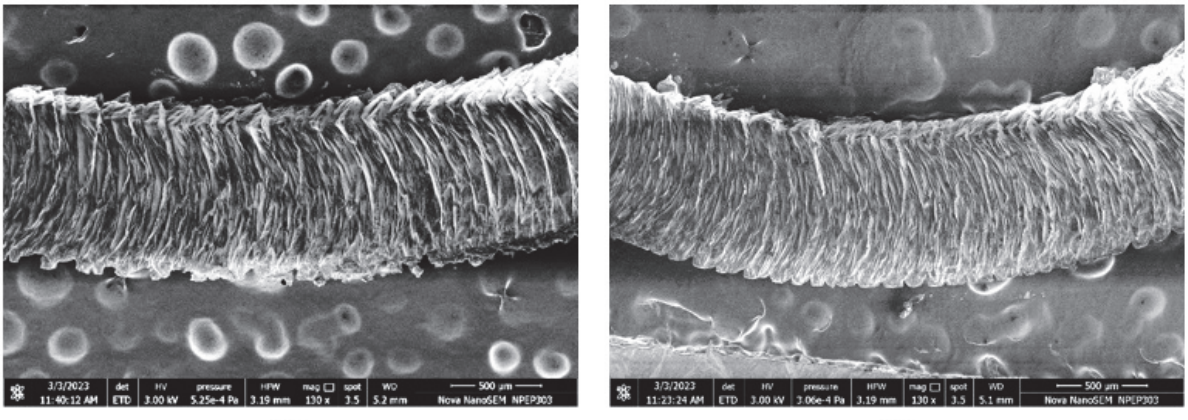

(a) (b)

Figure 11: SEM images of the chip's free surface at experiment index 6 for (a) Unitary nanofluid, (b) Hybrid nanofluid.

This study further observed chips with maximum serrations at higher cutting parameters, especially at higher cutting speeds and feed rates. It could be due to higher tool-chip interface friction and plastic deformation at higher cutting parameters. However, chips with lower serrations were observed with hybrid nanofluids, indicating their better lubrication and cooling

effects compared to unitary nanofluids. Hybrid nanofluids effectively remove heat from cutting zones due to superior cooling and lubricating capabilities, reducing friction between chips and tools, resulting in smooth-edged chips. It can be confirmed from Figs. 11(a) and (b), which show the free surfaces of chips produced with unitary and hybrid nanofluids, respectively. Hybrid nanofluids, containing MWCNTs and Al_2O_3, effectively prevent microparticle deposition on the chip's sliding surface by enhancing lubrication and cooling, respectively. It can be confirmed from Figs. 12(a) and (b), which show the back (sliding) surfaces of chips produced with unitary and hybrid nanofluids, respectively. The chips produced with hybrid nanofluid displayed polished sliding surfaces, while those with unitary nanofluid displayed rough sliding surfaces with parallel stripes and microdeposits, as shown in Figs. 11–12.

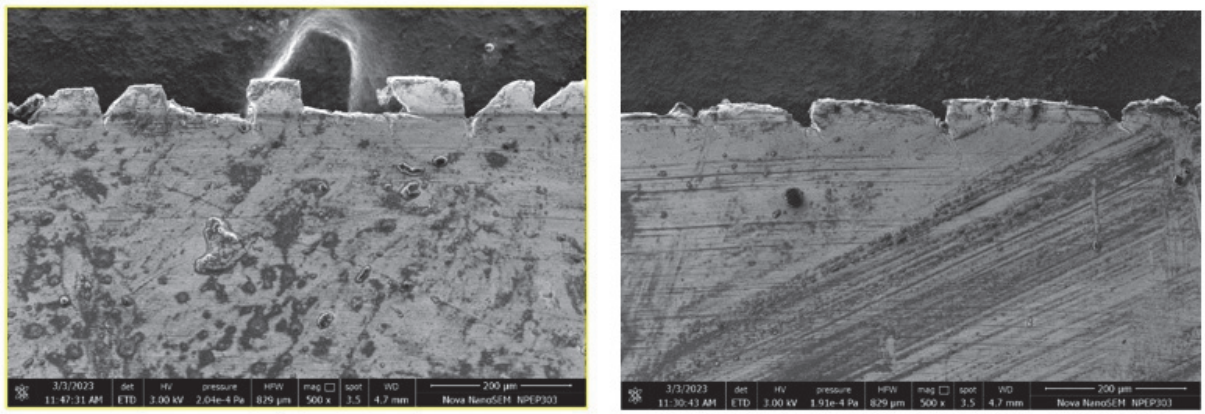

(a) (b)

Figure 12: SEM images of the chip's back or sliding surface at experiment index 6 for (a) Unitary nanofluid, (b) Hybrid nanofluid.

Figs. 13(a) and (b) display SEM images of the chip's free surface at experiment index 10 with unitary nanofluid for the worn-out tool and sharp tool. A sharp tool is a tool with practically zero tool wear, and a worn-out tool is a tool that has reached the end of its tool life. The severely damaged chip and non-uniform plastic deformation with abrasion marks on the free surface of the chip can be seen with the worn-out tool. Figs. 14(a) and (b) show SEM images of the chip's back or sliding surface at experiment index 10 with unitary nanofluid for the sharp tool and the worn-out tool, respectively. Deposition of the adhered particles and severe abrasion marks can be seen on the chip's back or sliding surface with the worn-out tool when using unitary nanofluids.

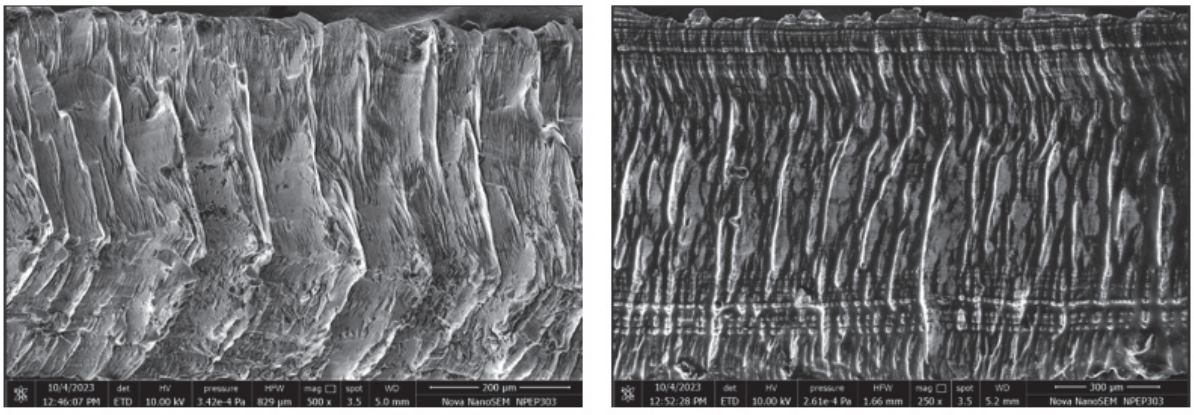

(a) (b)

Figure 13: SEM images of the chip's free surface at experiment index 10 with unitary nanofluid for (a) Sharp tool, (b) Worn-out tool.

Figs. 15 and 16 show SEM images of the chip's free and sliding surfaces at experiment index 10 with hybrid nanofluid for sharp tools and worn-out tools, respectively. A comparatively less damaged, uniform plastic deformation and no trace of any abrasion marks can be seen on the chip's free surface with the worn-out tool when using hybrid nanofluid. Moreover, chip morphology not significantly varying can be seen for the sharp and worn-out tool when using hybrid nanofluids.

However, there is a significant difference in the free and sliding surfaces of the chip when produced with a sharp and worn-out tool when using unitary nanofluid.

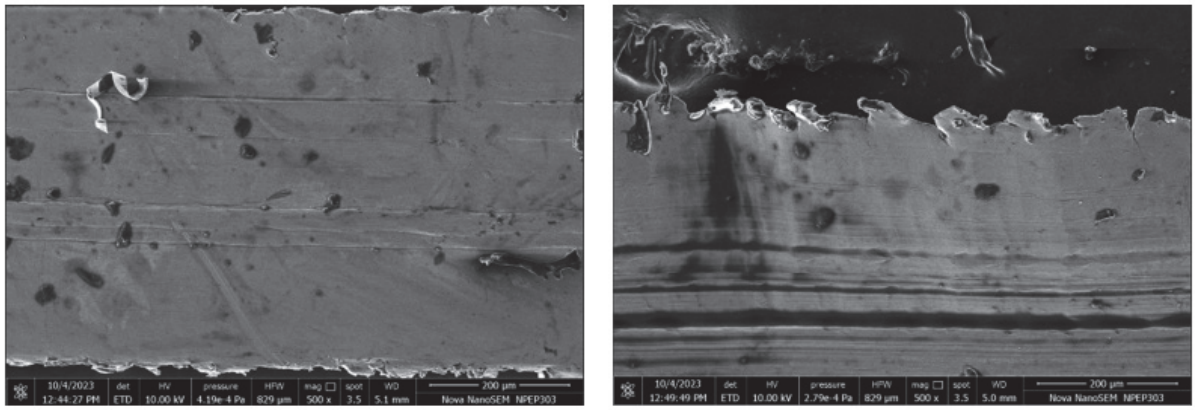

(a) (b)

Figure 14: SEM images of the chip's back surface at experiment index 10 with unitary nanofluid for (a) Sharp tool, (b) Worn-out tool.

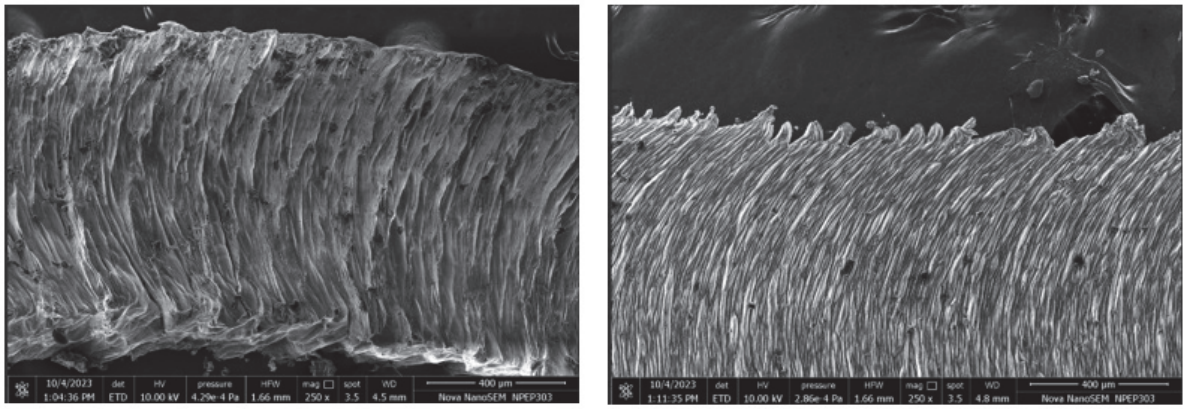

(a) (b)

Figure 15: SEM images of the chip's free surface at experiment index 10 with hybrid nanofluid for (a) Sharp tool, (b) Worn-out tool.

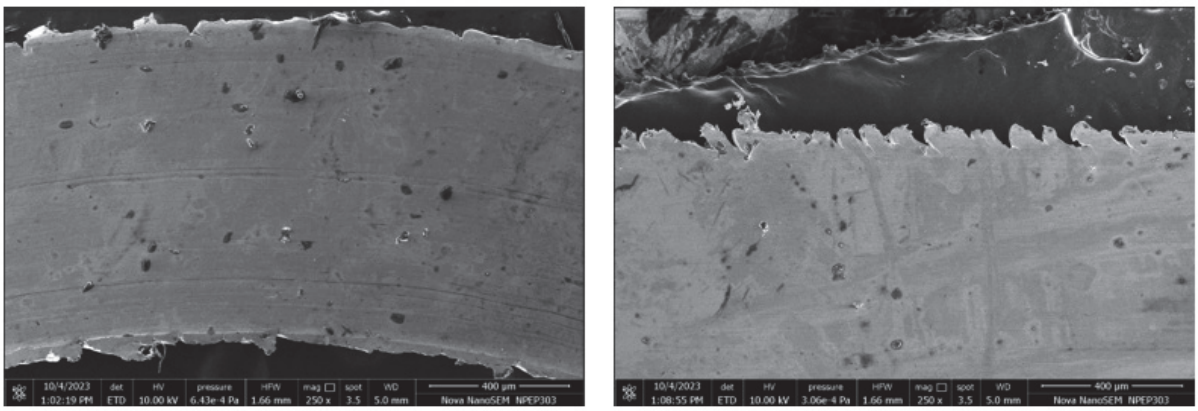

(a) (b)

Figure 16: SEM images of the chip's back surface at experiment index 10 with hybrid nanofluid for (a) Sharp tool, (b) Worn-out tool.

These findings confirm that the unitary nanofluid showed comparatively lower cooling effects, lower penetration, and wetting of less surface area compared to the hybrid nanofluid. It can also be confirmed by the higher values of surface

tension, wetting angle, and lower viscosity observed with the unitary nanofluid compared to the hybrid nanofluid, as depicted in Tab. 3.

The study demonstrates that a PVD-coated AlTiN tool with hybrid MWCNT+Al_2O_3 nanofluid provides a sustainable alternative for machining Inconel 718 alloy. Adding various nanoparticles to a base fluid to create hybrid nanofluids has been shown to be a viable method of improving machinability. Because using nanofluids under MQL conditions drastically lowers the amount of conventional cutting fluid used and minimizes waste production, it is consistent with sustainability goals. This study opens the door to further exploration and optimization of nanofluid-based MQL machining of Inconel 718 using evolutionary algorithms. Future research could address nanoparticle agglomeration and nanofluids' long-term stability.

Multi-objective optimization

Experimental investigations reveal that feed is more crucial than other cutting parameters for achieving better surface finish in turning Inconel 718 alloy under NFMQL conditions. By choosing a smaller feed and depth of cut and higher cutting speeds, one could achieve lower values of surface roughness and cutting forces. On the other hand, higher values for tool life could be obtained using lower values of cutting parameters. The objectives of having minimum surface roughness and cutting forces contradict the maximum tool life objective. It is therefore, important to perform a multi-objective optimization of process parameters that can simultaneously improve surface roughness, reduce cutting forces, and enhance tool life when turning Inconel 718 alloy using unitary and hybrid nanofluids under MQL.

The GA-TOPSIS provides the solution set that is the furthest from the NIS and the closest to the PIS. MATLAB is used to carry out a GA-based multi-objective optimization. The optimal solution from each set of solutions produced by a multi-objective genetic algorithm is found using TOPSIS. In MATLAB, a genetic optimization method is created using the objective functions Eqns. (11)-(15) for unitary nanofluids and Eqns. (16)-(20) for hybrid nanofluids. The range of process variables, such as V, f, and d, establishes the lower limits of the genetic optimization model, which has a lower bound of (30, 0.1, 0.2). The upper bound represents the upper limit of process parameters, set to (100, 0.3, 0.8).

The time limit, fitness limit, and stall time limit are all maintained infinitely to allow the optimizer to run. At 100, the stall generations are kept constant. Function and constraint tolerances are maintained at 10^{-4} and 10^{-3}, respectively, to get the best fit with the highest precision and the shortest computing time. Tolerance contributes to offering a variety of appropriate responses rather than aiming for the perfect response value. The GA optimizer is designed to run about 200 simulations before terminating on its own. The multi-objective genetic optimizer's other settings are left at their default settings. For the population type known as "Double Vector," this is the default option. To increase the likelihood of getting better outcomes, the tournament function is employed as a selection function, allowing all potential solutions to participate in the competition. Forward migration and intermediate crossover are the two forms of migration that are employed. The population's general variety and adaptability are facilitated by a mix of migration, crossover, and selection strategies.

After the optimization is completed, a collection of the most efficient and effective solutions that have been identified through the GA-algorithm process is acquired. The Pareto front, which shows all Pareto-efficient solutions in multi-objective optimization, is displayed in Tabs. 5 and 6 for unitary and hybrid nanofluids. The TOPSIS is applied to choose the ideal match among the outcomes of a multi-objective genetic algorithm. The unitary and hybrid nanofluids' normalized, weighted normalized values, PIS, NIS, separation measures, proximity coefficients, and rank are shown in Tabs. 7 and 8. According to GA-TOPSIS findings, the rank 1 optimal solution for run 7 with unitary nanofluid (Tab. 7) and run 5 with hybrid nanofluid (Tab. 8) both have excellent solutions.

Run No.	V (m/min)	f (mm/rev)	d (mm)	F_c (N)	F_f (N)	F_r (N)	R_a (μm)	T (min)
1	93.078	0.1	0.200	73.190	23.711	9.374	0.648	6.589
2	41.570	0.1	0.218	88.739	30.887	13.076	0.929	23.450
3	57.489	0.1	0.200	78.065	26.066	10.809	0.790	14.608
4	41.571	0.1	0.218	88.739	30.887	13.076	0.929	23.450
5	32.004	0.1	0.240	101.233	36.696	15.736	1.070	33.642
6	57.487	0.1	0.200	78.065	26.066	10.809	0.790	14.609
7	93.077	0.1	0.200	73.190	23.711	9.374	0.648	6.590
8	57.488	0.1	0.200	78.065	26.066	10.809	0.790	14.609
9	57.488	0.1	0.200	78.066	26.066	10.809	0.790	14.609
10	57.487	0.1	0.200	78.065	26.066	10.809	0.790	14.609

Table 5: Genetic algorithm: Pareto efficient solutions for unitary Al_2O_3 nanofluid.

Run No.	V (m/min)	f (mm/rev)	d (mm)	F_c (N)	F_f (N)	F_r (N)	R_a (µm)	T (min)
1	84.644	0.1	0.202	62.905	19.393	9.693	0.612	8.491
2	56.917	0.1	0.202	66.224	21.650	11.216	0.716	15.249
3	55.763	0.1	0.202	66.401	21.774	11.301	0.722	15.717
4	51.519	0.1	0.202	67.086	22.258	11.635	0.745	17.664
5	93.017	0.1	0.202	62.141	18.892	9.362	0.590	7.388
6	40.395	0.1	0.202	69.234	23.812	12.723	0.820	25.290
7	30.536	0.1	0.251	91.739	33.944	17.771	0.963	33.477
8	72.616	0.1	0.202	64.167	20.236	10.255	0.650	10.645

Table 6: Genetic algorithm: Pareto efficient solutions for hybrid Al_2O_3+MWCNT nanofluid.

Run no.	Normalized results for					Normalized weighted matrix for					Separation measures		Closeness coefficient	Rank
	F_c	F_f	F_r	R_a	T	F_c	F_f	F_r	R_a	T	S^+	S^-	CC_i	
1	15.3	4.7	1.7	0.11	0.54	0.53	0.29	0.15	0.009	0.402	10.077	0.699	0.935	2
2	22.5	8.0	3.4	0.24	6.90	0.78	0.50	0.29	0.019	5.091	5.399	4.702	0.535	9
3	17.4	5.7	2.3	0.17	2.67	0.60	0.36	0.20	0.014	1.976	8.504	1.681	0.835	3
4	22.5	8.0	3.4	0.24	6.90	0.78	0.50	0.29	0.019	5.091	5.399	4.702	0.535	8
5	29.3	11.^	4.9	0.32	14.2	1.01	0.71	0.43	0.025	10.47	0.699	10.07	0.065	10
6	17.4	5.7	2.3	0.17	2.68	0.60	0.36	0.20	0.014	1.976	8.504	1.681	0.835	7
7	15.3	4.7	1.7	0.11	0.54	0.53	0.29	0.15	0.009	0.402	10.077	0.699	0.935	1
8	17.4	5.7	2.3	0.17	2.67	0.60	0.36	0.20	0.014	1.976	8.504	1.681	0.835	4
9	17.4	5.7	2.3	0.17	2.68	0.60	0.36	0.20	0.014	1.976	8.504	1.681	0.835	5
10	17.4	5.7	2.3	0.17	2.68	0.60	0.36	0.20	0.014	1.976	8.504	1.681	0.835	6

Table 7: GA-TOPSIS ideal solutions ranking for unitary Al_2O_3 nanofluid.

The process parameters for optimum solutions can be referred to in Tabs. 5 and 6 for unitary and hybrid nanofluids, respectively. It has been seen that the cutting speed of 93 m/min, feed of 0.1 mm, and depth of cut of 0.2 mm are the ideal parameters for both nanofluids. With these parameters, the tangential cutting force of 79.19 and 62.141 N, feed force of 23.71 and 18.892 N, radial force of 9.374 and 9.362 N, surface roughness of 0.648 and 0.59 µm, and tool life of 6.59 and 7.388 minutes could be obtained during turning Inconel 718 alloy using unitary Al_2O_3 and hybrid Al_2O_3+MWCNT nanofluids under MQL conditions. However, to verify the accuracy of the findings, validation experiments must be conducted.

Run no.	Normalized results for					Normalized weighted matrix for					Separation measures		Closeness coefficient	Rank
	F_c	F_f	F_r	R_a	T	F_c	F_f	F_r	R_a	T	S^+	S^-	CC_i	
1	13.5	3.8	1.8	0.12	0.95	0.54	0.36	0.21	0.008	0.657	9.559	1.102	0.897	2
2	15.0	4.8	2.5	0.16	3.07	0.60	0.45	0.28	0.011	2.120	8.098	1.886	0.811	4
3	15.1	4.9	2.5	0.17	3.26	0.61	0.45	0.28	0.011	2.252	7.966	1.998	0.800	5
4	15.4	5.1	2.7	0.18	4.12	0.62	0.47	0.30	0.012	2.844	7.375	2.523	0.745	6
5	13.2	3.6	1.7	0.11	0.72	0.53	0.34	0.19	0.008	0.498	9.719	1.117	0.897	1
6	16.4	5.8	3.2	0.21	8.46	0.66	0.54	0.36	0.015	5.831	4.395	5.397	0.449	7
7	28.9	11.^	6.3	0.30	14.8	1.16	1.11	0.70	0.020	10.21	1.117	9.719	0.103	8
8	14.1	4.2	2.1	0.13	1.50	0.56	0.39	0.23	0.009	1.033	9.184	1.173	0.887	3

Table 8: GA-TOPSIS ideal solutions ranking for hybrid Al_2O_3+MWCNT nanofluid.

Tab. 9 presents a collection of GA-TOPSIS-obtained solutions for unitary and hybrid nanofluids. When utilizing unitary nanofluids, a greater tool life of 14.608 minutes with slightly higher values of cutting forces and surface roughness could be achieved with a cutting speed of 57.489 m/min, feed, and depth of cut of 0.1 mm/rev and 0.2 mm, respectively. However, the highest tool life of 17.664 minutes could be obtained using cutting speeds of 51.519 m/min, feed, and depth of cut of 0.1 mm/rev and 0.202 mm, respectively, when using hybrid nanofluids. A hybrid Al_2O_3+MWCNT nanofluid is a better option when turning Inconel 718 for obtaining better tool life, minimum cutting forces, and surface roughness.

Rank No.	V (m/min)	f (mm/rev)	d (mm)	F_c (N)	F_f (N)	F_r (N)	R_a (µm)	T (min)
Unitary Al_2O_3 nanofluid								
1	93.077	0.1	0.200	73.190	23.711	9.374	0.648	6.590
3	57.489	0.1	0.200	78.065	26.066	10.809	0.790	14.608
Hybrid Al_2O_3+MWCNT nanofluid								
1	93.017	0.1	0.202	62.141	18.892	9.362	0.590	7.388
2	84.644	0.1	0.202	62.905	19.393	9.693	0.612	8.491
3	72.616	0.1	0.202	64.167	20.236	10.255	0.650	10.645
4	56.917	0.1	0.202	66.224	21.650	11.216	0.716	15.249
5	51.519	0.1	0.202	67.086	22.258	11.635	0.745	17.664

Table 9: A collection of GA-TOPSIS-obtained solutions for unitary Al_2O_3 and hybrid Al_2O_3+MWCNT nanofluids.

Turning experiments are conducted using these ideal process parameters to obtain experimental validation of the optimized responses. The validation experiment was carried out at two different cutting conditions, as depicted in Tab. 10, with unitary and hybrid nanofluids. Tab. 10 compares the experimental findings at these ideal process parameters with the anticipated GA-TOPSIS responses. The values shown for cutting forces, surface roughness, and tool life are averages of measurements taken at three repeated trials for a tool, aiming to minimize outliers before analyzing the data. With an error of less than 10%, there is a good agreement between the answers from the optimization models and the experimental data at these ideal process parameters. It follows that these process parameter choices will provide the lowest possible cutting forces, surface roughness, and tool life.

Responses	Unitary Al_2O_3 nanofluid					Hybrid Al_2O_3+MWCNT nanofluid				
	GA-TOPSIS prediction	Experimental results (Repeated for three times)			Average % Error	GA-TOPSIS prediction	Experimental results (Repeated for three times)			Average % Error
		1st	2nd	3rd			1st	2nd	3rd	
V = 93 m/min, f = 0.1 mm/rev, d = 0.2 mm										
F_c (N)	73.19	80	84	68	9.73	62.14	67	59	71	8.56
F_f (N)	23.71	26	29	28	14.23	18.892	21	23	19	9.02
F_r (N)	9.37	10	11	8	12.80	9.362	10	11	9	9.42
R_a (µm)	0.648	0.7	0.64	0.71	5.77	0.59	0.65	0.62	0.54	7.96
T (min)	6.59	7.2	6.3	7.7	9.59	7.388	8.1	7.6	8.8	9.39
V = 57 m/min, f = 0.1 mm/rev, d = 0.2 mm										
F_c (N)	78.065	81	76	81	3.26	66.224	69	59	73	5.53
F_f (N)	26.066	23	27	28	5.18	21.65	23	24	25	6.26
F_r (N)	10.809	9.6	9.8	12	10.67	11.216	12	12.3	13	5.64
R_a (µm)	0.79	0.84	0.74	0.87	7.49	0.716	0.78	0.67	0.67	5.47
T (min)	14.608	13.4	13.9	15.6	6.96	15.249	16.2	13.4	14.1	6.74

Table 10: Validation experiments.

This study suggests the better machinability of Inconel 718 during turning using a PVD-coated AlTiN tool under NFMQL conditions with a cutting speed in the range of 50–70 m/min and a lower feed and depth of cut of 0.1 mm/rev and 0.2 mm,

respectively. However, prominent results could be obtained using a hybrid Al_2O_3+MWCNT nanofluid under MQL conditions. At these parameters, the tangential cutting force up to 80 N, surface roughness in the range of 0.6–0.7 μm, and tool life over 10 minutes could be obtained during turning Inconel 718 using nanofluids under NFMQL conditions.
This study finds that the Pareto-based hybrid GA-TOPSIS multi-objective optimization strategy ensured that the chosen compromise solution provided the best trade-off between conflicting objectives. GA provides a family of optimal solutions, and TOPSIS is used to rank these solutions based on their closeness to the ideal compromise solution. For a narrow range of process parameters, the GA-TOPSIS multi-objective optimization approach works well for faster solution retrieval because of its shorter computation time. This study suggests further research on the machining of Inconel 718 under NFMQL conditions, considering the machined surface integrity issues.

CONCLUSIONS

The machining of nickel alloys severely damages cutting tools because of their low heat conductivity and poor machinability, which raises manufacturing costs. With this view, this study evaluates the machining performance during turning Inconel 718 using unitary and hybrid nanofluids under minimum quantity lubrication (NFMQL). The study investigated the machining effects of dispersed unitary and hybrid nanofluids under MQL on cutting force, surface roughness, chip morphology, tool life, and tool wear. The nanofluid was prepared using palm oil by dispersing Al_2O_3 nanoparticles (unitary nanofluid) and Al_2O_3+MWCNT nanoparticles (hybrid nanofluid). The process parameters were optimized for optimum machining performance by combining the Pareto-based genetic algorithm and TOPSIS (GA-TOPSIS) multi-objective optimization strategy. From the current study, the following conclusions could be drawn:

- This study suggests the better machinability of Inconel 718 alloy during turning using a PVD-coated AlTiN tool under NFMQL conditions with a cutting speed in the range of 50–70 m/min and a lower feed and depth of cut of 0.1 mm/rev and 0.2 mm, respectively. However, prominent results could be obtained using a hybrid Al_2O_3+MWCNT nanofluid under MQL conditions. At these parameters, the tangential cutting force up to 80 N, surface roughness in the range of 0.6–0.7 μm, and tool life over 10 minutes could be obtained during turning Inconel 718 alloy using unitary Al_2O_3 and hybrid Al_2O_3+MWCNT nanofluids under MQL conditions.
- Hybrid nanofluid performed better than unitary nanofluid in terms of reduced cutting forces, surface roughness, and improved tool life due to the combined effects of the higher viscosity and lower surface tension of MWCNTs and the higher thermal conductivity and lower contact angle of Al_2O_3 nanoparticles.
- The built-up edge formation and adhesion wear were significant wear mechanisms when turning Inconel 718 with PVD-coated tools using unitary and hybrid nanofluids under MQL conditions.
- The chips produced with hybrid nanofluid displayed polished sliding surfaces, while those with unitary nanofluid displayed rough sliding surfaces with parallel stripes and microdeposits. Moreover, hybrid nanofluids effectively remove heat from cutting zones due to their superior cooling and lubricating capabilities, reducing friction between chips and tools, and resulting in smooth-edged chips.
- The chip's morphology significantly changed with sharp and worn-out tools, most prominently with unitary nanofluids. On the other hand, when using hybrid nanofluid, the chip's free surface showed no signs of abrasion marks and a much less damaged, uniform plastic deformation.
- The Pareto-based hybrid GA-TOPSIS multi-objective optimization strategy allowed for the identification of optimal cutting parameters that ensured an efficient and effective decision-making process for determining the best cutting parameters.

REFERENCES

[1] Khanna, N., Agrawal, C., Dogra, M. and Pruncu, C.I. (2020). Evaluation of tool wear, energy consumption, and surface roughness during turning of inconel 718 using sustainable machining technique. J. Mater. Res. Technol., 9(3), pp. 5794-5804. DOI: 10.1016/j.jmrt.2020.03.104

[2] Kulkarni, P. and Chinchanikar, S. (2023). A Review on Machining of Nickel-Based Superalloys Using Nanofluids Under Minimum Quantity Lubrication (NFMQL). J. Inst. Eng. India Ser. C, 104(1), pp. 183-199. DOI: 10.1007/s40032-022-00905-w

[3] Matos, F., Silva, T.E.F., Marques, F., Figueiredo, D., Rosa, P. A.R. and de Jesus, A.M.P. (2023). Machinability assessment of Inconel 718 turning using PCBN cutting tools. Procedia CIRP, 117, pp. 468-473. DOI: 10.1016/j.procir.2023.03.079
[4] Airao, J., Khanna, N. and Nirala, C.K. (2022). Tool wear reduction in machining Inconel 718 by using novel sustainable cryo-lubrication techniques. Tribol. Int., 175, p. 107813. DOI: 10.1016/j.triboint.2022.107813
[5] Rajurkar, A. and Chinchanikar, S. (2023). Investigations on homothetic and hybrid micro-textured tools during turning Inconel-718. Mater. Manuf. Processes, pp. 1-17. DOI: 10.1080/10426914.2023.2236188
[6] Rajurkar, A. and Chinchanikar, S. (2022). Experimental Investigation on Laser-Processed Micro-Dimple and Micro-Channel Textured Tools during Turning of Inconel 718 Alloy. J. Mater. Eng. Perform., 31(5), pp. 4068-4083. DOI: 10.1007/s11665-021-06493-7
[7] Rajurkar, A. and Chinchanikar, S. (2023). Investigation on the effect of laser parameters and hatch patterns on the dimensional accuracy of micro-dimple and micro-channel texture geometries, Int. J. Interact. Des. Manuf., pp. 1-18. DOI: 10.1007/s12008-023-01258-z
[8] Chinchanikar, S., Kore, S. S. and Hujare, P. (2021). A review on nanofluids in minimum quantity lubrication machining. J. Manuf. Processes, 68, pp. 56-70. DOI: 10.1016/j.jmapro.2021.05.028
[9] Pandey, K. and Datta, S. (2021). Machinability study of Inconel 825 superalloy under nanofluid MQL: Application of sunflower oil as a base cutting fluid with MWCNTs and nano-Al_2O_3 as additives. In Sustainable Manufacturing and Design. Woodhead Publishing, pp. 151-197.
[10] Şirin, Ş., Sarıkaya, M., Yıldırım, Ç.V. and Kıvak, T. (2021). Machinability performance of nickel alloy X-750 with SiAlON ceramic cutting tool under dry, MQL and hBN mixed nanofluid-MQL. Tribol. Int., 153, p. 106673. DOI: 10.1016/j.triboint.2020.106673
[11] Faheem, A., Husain, T., Hasan, F. and Murtaza, Q. (2022). Effect of nanoparticles in cutting fluid for structural machining of Inconel 718. Adv. Mater. Process. Technol., 8(1), pp. 259-276.
[12] Sharma, V.K., Singh, T., Singh, K., Rana, M., Gehlot, A. and Verma, R. (2023). Influence of hybrid nanofluid on tool wear and surface roughness in MQL-assisted face milling of AISI 52100. Adv. Mater. Process. Technol., pp. 1-12.
[13] Bahedh, A.S., Mishra, A., Al-Sabur, R., Jassim, A.K. (2022). Machine learning algorithms for prediction of penetration depth and geometrical analysis of weld in friction stir spot welding process. Metall. Res. Technol., 119(3), p. 305. DOI: 10.1051/metal/2022032
[14] Ikram, K., Djilali, K., Abdennasser, D., Al-Sabur, R., Ahmed, B., Sharkawy, A.N. (2023). Comparative analysis of fouling resistance prediction in shell and tube heat exchangers using advanced machine learning techniques. Res. Eng. Struct. Mater. DOI: 10.17515/resm2023.858en0816
[15] Senthilkumar, K.M., Thirumalai, R., Selvam, T.A., Natarajan, A. and Ganesan, T. (2021). Multi objective optimization in machining of Inconel 718 using taguchi method. Mater. Today Proc., 37, pp. 3466-3470. DOI: 10.1016/j.matpr.2020.09.333
[16] Hegab, H., Salem, A., Rahnamayan, S. and Kishawy, H.A. (2021). Analysis, modeling, and multi-objective optimization of machining Inconel 718 with nano-additives based minimum quantity coolant. Appl. Soft Comput., 108, p. 107416. DOI: 10.1016/j.asoc.2021.107416
[17] Elsheikh, A.H., Muthuramalingam, T., Shanmugan, S., Ibrahim, A.M.M., Ramesh, B., Khoshaim, A.B., ... and Sathyamurthy, R. (2021). Fine-tuned artificial intelligence model using pigeon optimizer for prediction of residual stresses during turning of Inconel 718. J. Mater. Res. Technol., 15, pp. 3622-3634. DOI: 10.1016/j.jmrt.2021.09.119
[18] Satyanarayana, B., Yadav, G.S.G., Nitin, P.R. and Reddy, M.D. (2015). Simultaneous optimization of multi performance characteristics in dry turning of Inconel 718 using NSGA-II. Mater. Today Proc., 2(4-5), pp. 2423-2432. DOI: 10.1016/j.matpr.2015.07.182
[19] Pawade, R.S. and Joshi, S.S. (2011). Multi-objective optimization of surface roughness and cutting forces in high-speed turning of Inconel 718 using Taguchi grey relational analysis (TGRA). Int. J. Adv. Manuf. Technol., 56, pp. 47-62. DOI: 10.1007/s00170-011-3183-z
[20] Thirumalai, R., Seenivasan, M. and Panneerselvam, K. (2021). Experimental investigation and multi response optimization of turning process parameters for Inconel 718 using TOPSIS approach. Mater. Today Proc., 45, pp. 467-472. DOI: 10.1016/j.matpr.2020.02.004
[21] Zhou, J., Ren, J. and Yao, C. (2017). Multi-objective optimization of multi-axis ball-end milling Inconel 718 via grey relational analysis coupled with RBF neural network and PSO algorithm. Measurement, 102, pp. 271-285. DOI: 10.1016/j.measurement.2017.01.057
[22] Sen, B., Mia, M., Mandal, U.K., Dutta, B. and Mondal, S.P. (2019). Multi-objective optimization for MQL-assisted end milling operation: an intelligent hybrid strategy combining GEP and NTOPSIS. Neural Comput. Appl., 31, pp. 8693-8717. DOI: 10.1007/s00521-019-04450-z

[23] Hwang, Y.J., Lee, J. K., Lee, C.H., Jung, Y.M., Cheong, S.I., Lee, C.G., and Jang, S.P. (2007). Stability and thermal conductivity characteristics of nanofluids. Thermochim. Acta, 455(1-2), pp. 70-74. DOI: 10.1016/j.tca.2006.11.036
[24] Chinchanikar, S., Shinde, S., Shaikh, A., Gaikwad, V. and Ambhore, N.H. (2023). Multi-objective Optimization of FDM Using Hybrid Genetic Algorithm-Based Multi-criteria Decision-Making (MCDM) Techniques. J. Inst. Eng. India Ser. D. DOI: 10.1007/s40033-023-00459-w
[25] Chinchanikar, S., Katiyar, J.K. and Manav, O. (2022). Multi-objective optimization of turning of titanium alloy under minimum quantity lubrication. Journal of Optimization in Industrial Engineering, 15(1), pp. 243-260. DOI: 10.22094/JOIE.2021.1937743.1886
[26] Pavić, Z. and Novoselac, V. (2013). Notes on TOPSIS method. Int. J. Res. Eng. Sci., 1(2), pp. 5–12.
[27] Sakthivel, G., Ilangkumaran, M. and Gaikwad, A. (2015). A hybrid multicriteria decision modeling approach for the best biodiesel blend selection based on ANP-TOPSIS analysis. Ain. Shams. Eng. J., 6(1), pp. 239–256. DOI: 10.1016/j.asej.2014.08.003
[28] Wu, J., Li, P., Qian, H. and Chen, J. (2015). On the sensitivity of entropy weight to sample statistics in assessing water quality: statistical analysis based on large stochastic samples. Environ. Earth Sci., 74(3), pp. 2185–2195. DOI: 10.1007/s12665-015-4208-y
[29] Yan, F., Qian, B. and Xiao, X. (2019). Geo-accumulation vector model for evaluating the heavy metal pollution in the sediments of Western Dongting Lake. J. Hydrol., 567(7), pp. 112–124. DOI: 10.1016/j.jhydrol.2019.03.064
[30] Yan, F., Qiao, D.Y. and Qian, B. (2019). Improvement of CCME WQI using grey relational method. J. Hydrol., 543(2), pp. 316–323. DOI: 10.1016/j.jhydrol.2016.10.007
[31] Gorgij, A.D., Kisi, O., Moghaddam, A.A. and Taghipour, A. (2017). Groundwater quality ranking for drinking purposes, using the entropy method and the spatial autocorrelation index. Environ. Earth Sci., 76, p. 9. DOI: 10.1007/s12665-017-6589-6
[32] Li, X.G., Wei, X. and Huang, Q. (2012). Comprehensive entropy weight observability-controllability risk analysis and its application to water resource decision-making. Water SA, 38, pp. 573–579. DOI: 10.4314/wsa.v38i4.13
[33] Dong, G.H., Shen, J.Q., Jia, Y.Z. and Sun, F.H. (2018). Comprehensive evaluation of water resource security: case study from Luoyang City, China. Water, 10, p. 19. DOI: 10.3390/w10081106
[34] Amiri, V., Rezaei, M. and Sohrabi, N. (2014). Groundwater quality assessment using entropy weighted water quality index (EWQI) in Lenjanat, Iran. Environ. Earth Sci., 72(9), pp. 3479–3490. DOI: 10.1007/s12665-014-3255-0
[35] Sarkar, S. and Datta, S. (2021). Machining performance of Inconel 718 under dry, MQL, and nanofluid MQL conditions: application of coconut oil (base fluid) and multi-walled carbon nanotubes as additives. Arabian J. Sci. Eng., 46, pp. 2371-2395. DOI: 10.1007/s13369-020-05058-5
[36] Pawade, R.S. and Joshi, S.S. (2011). Mechanism of chip formation in high-speed turning of Inconel 718. Mach. Sci. Technol., 15(1), pp. 132-152. DOI: 10.1080/10910344.2011.557974
[37] Jawahir, I.S. and Van Luttervelt C.A. (1993). Recent developments in chip control research and applications. CIRP Ann., 42(2), 659-693. DOI: 10.1016/S0007-8506(07)62531-1
[38] Abbasi, S.A. and Pingfa, F. (2015). Evaluating the effectiveness of various coating layers applied on k-grade cemented carbide cutting tools on machinability of titanium alloy Ti-6Al-4V in high speed end milling. In2015 12th International Bhurban Conference on Applied Sciences and Technology (IBCAST) 2015 Jan 13 (pp. 14-19). IEEE. DOI: 10.1109/IBCAST.2015.7058472
[39] Rakesh, M. and Datta, S. (2020). Machining of Inconel 718 using coated WC tool: effects of cutting speed on chip morphology and mechanisms of tool wear. Arabian J. Sci. Eng., 45(2), pp. 797-816. DOI: 10.1007/s13369-019-04171-4